Published in final edited form as:
Methods Cell Biol. 2015 ; 127: 509–542. doi:10.1016/bs.mcb.2014.12.011.

Scanning and three-dimensional electron microscopy methods for the study of *Trypanosoma brucei* and *Leishmania mexicana* flagella

Eva Gluenz[*], **Richard John Wheeler**[*], **Louise Hughes**[§], and **Sue Vaughan**[§,1]

[*]Sir William Dunn School of Pathology, University of Oxford, Oxford, UK

[§]Department of Biological and Medical Sciences, Oxford Brookes University, Oxford, UK

Abstract

Three-dimensional electron microscopy tools have revolutionized our understanding of cell structure and molecular complexes in biology. Here, we describe methods for studying flagellar ultrastructure and biogenesis in two unicellular parasites—*Trypanosoma brucei* and *Leishmania mexicana*. We describe methods for the preparation of these parasites for scanning electron microscopy cellular electron tomography, and serial block face scanning electron microscopy (SBFSEM). These parasites have a highly ordered cell shape and form, with a defined positioning of internal cytoskeletal structures and organelles. We show how knowledge of these can be used to dissect cell cycles in both parasites and identify the old flagellum from the new in *T. brucei*. Finally, we demonstrate the use of SBFSEM three-dimensional models for analysis of individual whole cells, demonstrating the excellent potential this technique has for future studies of mutant cell lines.

INTRODUCTION

The family Trypanosomatidae contains a number of human-infective protozoan parasites, which collectively pose major public health problems in many parts of the world. These include *Trypanosoma brucei*, which causes African sleeping sickness, *Trypanosoma cruzi*, causing Chagas disease in Central and South America, and species of *Leishmania* that cause leishmaniasis in many subtropical and tropical areas of the world (Stuart et al., 2008). Trypanosomatids are a monophyletic sister group to free-living eubodonids (Deschamps et al., 2011) and despite the marked differences in disease pathology caused by trypanosomatid parasites, trypanosomes and *Leishmania* spp. share interesting biological features. Both have a digenetic life cycle and different life cycle stages are characterized by distinctive morphologies (Hoare & Wallace, 1966; Vickerman, Tetley, Hendry, & Turner, 1988) (Figure 1). Common to all trypanosomatid cell architectures is the possession of a single flagellum. The flagellum, together with the rest of the strictly defined cell architecture and cell organelles, has to be replicated once during each cell cycle. Unlike the situation for cilia in mammalian cells, the trypanosomatid flagellum is not disassembled prior to cell division;

[1]Corresponding author: svaughan@brookes.ac.uk.

Europe PMC Funders Author Manuscripts

it remains intact and a new flagellum is built alongside the old (Sherwin & Gull, 1989). The flagellum is interesting to study in these parasites for a number of reasons. It is important for parasite pathogenicity and in trypanosomes is critical for motility in mammalian blood, traversing the insect vector, attachment to the insect vector, and key roles in cell morphogenesis (Engstler et al., 2007; Ralston, Kabututu, Melehani, Oberholzer, & Hill, 2009; Rotureau, Ooi, Huet, Perrot, & Bastin, 2014; Sharma et al., 2008; Sherwin & Gull, 1989). These parasites have also emerged as genetically tractable model organisms for the study of conserved features of eukaryotic cilia and flagella and evolutionary cell biology (Akiyoshi & Gull, 2013; van Dam et al., 2013; Hoog et al., 2014; McKean, Baines, Vaughan, & Gull, 2003; Molla-Herman et al., 2010; Morga & Bastin, 2013; Wideman, Leung, Field, & Dacks, 2014).

During the life cycle of *T. brucei* (Figure 1(A)) the parasite alternates between dividing forms and nondividing forms. *T. brucei* remains extracellular throughout its life cycle, unlike *Leishmania* spp. and *T. cruzi*, which both live in an intracellular environment within mammalian hosts (Matthews, 2005). All of the life cycle stages are flagellated, but the size and shape of each life cycle stage differs and identification of the different life cycle forms has traditionally been achieved using key morphological characteristics (Hoare & Wallace, 1966; Vickerman, 1985). In *T. brucei* a single flagellum exits the flagellar pocket close to the posterior end of the cell and is attached along the length of the tubular-shaped cell body, with a short distal portion of the flagellum extending from the anterior end of the cell body (Figures 1(A) and 3(A)) (Sherwin & Gull, 1989; Vickerman, 1969b). The basal body is located at the proximal end of the flagellum close to the flagellar pocket with a probasal body lying alongside. Physically attached to the basal bodies is the kinetoplast, a structure that contains the mitochondrial DNA which is a unique characteristic of the order Kinetoplastida to which these parasites belong (Figure 4) (Lukes, Hashimi, & Zikova, 2005; Robinson & Gull, 1991; Robinson, Sherwin, Ploubidou, Byard, & Gull, 1995). The flagellum has a canonical 9 + 2 axoneme (9 outer doublet microtubules and 2 central pair microtubules) and an additional lattice-like structure attached to outer doublets 4 through 7 called the paraflagellar rod (PFR) (Figure 2(A)) (Gull, 1999; Hughes, Ralston, Hill, & Zhou, 2012). The precise function of this extraaxonemal structure is not fully understood, but failure to fully assemble a PFR results in loss of motility (Bastin, Sherwin, & Gull, 1998; Hill, 2003). The flagellum is attached along the length of the cell body by a flagellum attachment zone (FAZ). This is composed of filaments and a set of four specialized rootlet microtubules called the microtubule quartet (MtQ) (Hoog, Bouchet-Marquis, McIntosh, Hoenger, & Gull, 2012; Kohl, Sherwin, & Gull, 1999). The MtQ originates at the proximal end of the flagellum between the basal body pair and extends around the flagellar pocket, inserting into the subpellicular array of microtubules that are located beneath the cell body membrane (Figures 1(A) and 8(B)) (Lacomble et al., 2009).

Leishmania spp. share with trypanosomes many of the distinctive features of the trypanosomatid cell architecture described above. Their overall cell shape is determined by the array of subpellicular microtubules that underlies the plasma membrane. A single flagellum emerges from a flagellar pocket, located in *Leishmania* at the anterior end of the cell, and the base of the flagellum is anchored to the kinetoplast DNA complex. During the

course of their life cycle, *Leishmania* spp. alternate between two morphological forms, the small round amastigote forms, which replicate in the mammalian host, and the elongated promastigote forms that live in the phlebotomid sandfly vector. Following ingestion of amastigotes by a blood-feeding sandfly, the parasites progress through a series of distinct promastigote morphologies, alternating between replicating and nonreplicating stages (Gossage, Rogers, & Bates, 2003; Rogers, Chance, & Bates, 2002) (Figure 1(B)). The flagellum of promastigotes is long and motile, with a canonical 9 + 2 axoneme structure and extra-axonemal PFR (Figure 7(C) and (D)). Like the *T. brucei* flagellum, it is used for motility and attachment in the insect vector. Ultrastructural studies of the mode of flagellar attachment of *Leishmania mexicana amazonensis* in *Lutzomyia longipalpis* showed that slender nondividing nectomonad forms are found with their flagella inserted between the microvilli of the posterior midgut, without the formation of junctional complexes. In the esophageal valve, broad haptomonad forms are attached to the cuticular lining via their flagellar tips, forming hemidesmosomes (Killick-Kendrick, Molyneux, & Ashford, 1974). It has been proposed that haptomonad promastigotes may represent an “altruistic” life cycle stage (Bates, 2007) that, together with the plug formed by the parasite-secreted filamentous proteophosphoglycan, contributes to a blockage of the esophagus, which alters the feeding behavior of the sandfly and enhances parasite transmission (Rogers, Ilg, Nikolaev, Ferguson, & Bates, 2004). The precise position of haptomonad promastigotes in the developmental progression from procyclic to metacyclic promastigotes is unclear and the mechanisms involved in modulating flagellar structure and molecular interactions between the flagellar tip of the parasite and the chitin lining of the valve await further characterization. The flagellum of *Leishmania* promastigotes is not attached to the cell body beyond the exit point from the flagellar pocket and other than linkage to the kinetoplast, no function of the promastigote flagellum in cell morphogenesis has been demonstrated. The average flagellum length of promastigote forms increases progressively as they develop from procyclic forms into nectomonad, leptomonad, and finally metacyclic forms (Figure 1(B)). The most striking feature of the *Leishmania* flagellum is that when the metacyclic promastigote form, with its long motile flagellum, enters mammalian phagocytes it transforms into an amastigote form with a short nonmotile flagellum that structurally resembles primary cilia of mammalian cells (Gluenz, Hoog, et al., 2010). The reverse process occurs when amastigote forms taken up by a sandfly transform back to promastigotes (Gadelha, Cunha-e-Silva, & de Souza, 2013). The *Leishmania* flagellum thus offers opportunities to study the control of flagellum length and modulation of axoneme structure.

1.RATIONALE

This chapter seeks to provide methods on the use of three-dimensional electron microscopy methods to study flagella in *T. brucei* and *Leishmania* spp. and describes how these methods have been used to elucidate some important morphogenetic events during the cell and life cycle of *T. brucei* and *L. mexicana*. We describe cytological markers that aid in the identification of cell cycle stages and cellular orientation. The ability to recognize these facilitates analysis of micrographs of wild-type cells as well as interpretation of mutant phenotypes.

2. METHODS

2.1 IDENTIFICATION OF FLAGELLUM AGE AND CELL CYCLE STAGES IN *T. BRUCEI*—

There are a number of ultrastructural cytological characteristics that allow identification of the new flagellum and the old flagellum throughout the cell division cycle. In trypanosomes, the old flagellum remains intact and attached to the cell body during the cell division cycle with the new flagellum growing alongside and there is strict cytological positioning of the old flagellum relative to the new flagellum, which facilitates identification of the old and new flagellum in electron micrographs. In scanning electron microscopy (SEM) images the new flagellum is always located to the left of the old flagellum when viewed from posterior toward anterior during growth of the new flagellum (Figure 3(C)) (Wheeler, Scheumann, Wickstead, Gull, & Vaughan, 2013). By transmission electron microscopy (TEM) there are a number of ultrastructural features that can be used to differentiate the old flagellum from the new flagellum. The MtQ is always located to the left of the FAZ filament in TEM cross sections of flagella when viewed from posterior to anterior (Figure 2(A)) (Vaughan, Shaw, & Gull, 2006). They are the only microtubules underlying the cell body membrane with endoplasmic reticulum closely associated (Figure 2(A)) (Lacomble, Vaughan, Deghelt, Moreira-Leite, & Gull, 2012; Vickerman, 1969a). In this orientation the outer dynein arms on the nine outer doublets of the axoneme are in a clockwise orientation and the new flagellum is positioned to the left of the old flagellum (Figure 2(B) and (C)). Ultrastructural studies have been very important in enabling a detailed dissection of flagellar structures and function in *T. brucei* and have enabled comparisons to be made between the old and new flagellum. This was used in the identification of the ponticulus, a bridge-like structure within the B-tubule of all nine outer doublet microtubules. Analysis of cross sections though old and new flagella demonstrated that ponticuli were only present in the old flagellum and not in the growing new flagellum (Vaughan et al., 2006) (Figure 2(B) and (C)).

The strict cytological positioning is defined by the cytoskeleton, which consists of a planar array of microtubules underlying the plasma membrane (Hemphill, Lawson, & Seebeck, 1991). These are cross-linked to each other and the plasma membrane with the plus ends facing the posterior end of the cell (Gull, 1999). During the cell division cycle the cytoarchitecture remains intact and two new daughters form within the confines of the existing cytoskeleton. This necessitates a highly ordered duplication and segregation of cellular structures and organelles. The cell division cycle of *T. brucei* is well characterized and defined spatio-temporal duplication and segregation of a number of single copy organelles makes it possible to easily identify cell cycle stages by microscopy and follow assembly of the new flagellum during cell division (Sherwin & Gull, 1989) (Figure 4). Trypanosomes are unusual in having the mitochondrial DNA condensed within the kinetoplast (called kinetoplast DNA) (Vickerman, 1985) and this allows identification of both the DNA of the nucleus and mitochondrial DNA in cells stained with DNA intercalating dyes such as 4′,6-diamidino-2-phenyl-indole (DAPI). Analysis of DNA replication timings using 5-bromo-2-deoxyuridine-substituted DNA has demonstrated there to be separate periodic replication and segregation timings for each genome (Woodward & Gull, 1990) (Figure 4) providing precise temporal markers of cell cycle progression. Cells in G1 contain a single kinetoplast, nucleus, and single flagellum and are referred to as 1K1N (1

kinetoplast 1 nucleus) cells. Initiation of the S-phase of the kinetoplast DNA coincides with basal body duplication and marks the beginning of new flagellum assembly (Woods et al., 1989). The new flagellum extends into the existing flagellar pocket and while in the pocket it rotates anticlockwise around the old flagellum. This rotation is required to set up the strict cytological positioning so that once the new flagellum exits the flagellar pocket it is positioned to the left of the old flagellum (Figure 8) (Lacomble et al., 2009, 2010)—see Section 3.7. As the new flagellum extends in length the distance between the basal bodies increases (Robinson et al., 1995) and consequently the duplicated kinetoplasts, which are physically attached to the basal bodies, segregate, leading to a 2K1N configuration. Mitosis proceeds to give a 2K2N configuration, followed by cytokinesis (Figure 4) (Sherwin & Gull, 1989).

2.2 CELL CULTURE

2.2.1 Procyclic form *T. brucei brucei*: The procylic form is one of the insect forms that proliferate in the midgut of tsetse flies. There are a number of culture-adapted strains. In our studies we use Lister 427. This form is grown in a semidefined SDM-79 medium (Brun & Schonenberger, 1979) which is supplemented with 10% (v/v) heat-inactivated fetal bovine serum (FBS) and grown at 28 °C in phenolic cap tissue culture flasks. The cells should be kept between 10^6 and 10^7 cells/mL for optimum exponential growth. Above this concentration the cells enter a stationary phase. Cells are routinely harvested for electron microscopy studies at 5×10^6 to 8×10^6 cells/mL.

2.2.2 Bloodstream form *T. brucei brucei*: The bloodstream form is the proliferating life cycle form in the mammalian bloodstream. We use strain Lister 427 in our SEM studies. This form is grown in a semi-defined HMI-9 medium supplemented with 15% (v/v) heat-inactivated FBS and grown at 37 °C in a 5% CO_2 incubator in vented top culture flasks (Hirumi & Hirumi, 1994). This cell type should be grown at a lower concentration than procyclic form cells and harvested at ~8×10^5 cells/mL for microscopy studies. All *T. brucei* cell line stocks are stored in liquid nitrogen in medium supplemented with 10% glycerol. Cells are sensitive to different batches of FBS, which should be tested before use.

2.2.3 *L. mexicana* culture: Promastigote-form *L. mexicana* (WHO strain MNYC/BZ/62/M379) are grown at 28 °C in M199 medium supplemented with 26 mM $NaHCO_3$, 7.7 μM hemin, 40 mM 4-(2-hydroxyethyl)piperazine-1-ethanesulfonic acid (HEPES) pH 7.4, and 10% (v/v) FBS. Batches of FBS should be tested before use. Maintaining cultures between 10^6 and 10^7 cells/mL ensures continuous exponential growth. For electron microscopy studies, promastigotes should be harvested at a density of ~5 8×10^6 to $\times 10^6$ cells/mL. Axenic amastigotes are generated by a subculture of promastigote forms into Schneider's *Drosophila* medium supplemented with 20% (v/v) FBS and 25 mM 4-morpholineethanesulfonic acid sodium salt (MES)·HCl pH 5.5 and incubation at 34 °C in a 5% CO_2 incubator in vented top culture flasks (Bates, 1994).

2.3 PREPARATION OF CELLS FOR SEM

2.3.1 Primary fixation of cells for SEM: Fixation should ideally be carried out in the suspension culture in order to minimize manipulation of cells prior to fixation. This is

achieved by the addition of EM-grade glutaraldehyde directly to the suspension culture flask, straight out of the incubator, to a final concentration of 2.5% glutaraldehyde (from a 25% stock of EM-grade glutaraldehyde). A 50 mL culture of cells is sufficient for ~10 coverslips. The fixed cell suspension should then be moved to a 50 mL falcon tube and centrifuged for 10 min at 800 g. The supernatant is removed and cells resuspended in primary fixative of 2.5% EM-grade glutaraldehyde in phosphate-buffered saline (PBS) for 2 h at room temperature on a rocking stage set to a low setting.

2.3.2 Settling cells on coverslips: Once the cells have been fixed they need to be settled onto coverslips; we routinely use 13 mm round glass coverslips. We have found that life cycle forms differ in their adherence properties and require different coatings of coverslip. The *T. brucei* procyclic form and *L. mexicana* amastigote form adhere to glass coverslips without any additional coating. The *L. mexicana* promastigote forms adhere better to poly-L-lysine-coated glass. To coat coverslips the glass should be cleaned with ethanol, followed by immersion in a 0.1% (w/v) solution of poly-L-lysine in water. Coverslips are then rinsed in water and left to air-dry. Alternatively, poly-L-lysine-coated coverslips can be purchased commercially. The bloodstream form *T. brucei* cells do not adhere to either glass or poly-L-lysine-coated coverslips. We found that they adhere well to Thermanox (Thermo Scientific) coverslips, which are also suitable for adherence of procyclic form *T. brucei*. Before settling onto coverslips, it is essential that cells are washed 2–3 times in PBS to remove the culture medium otherwise the cells will not adhere to any of the coverslips. To wash the 50 mL culture of cells, they should be centrifuged for 10 min at 800 g. Remove as much of the supernatant as possible and add half the volume of PBS. Centrifuge once more and then resuspend the pellet in PBS to half of the original volume (~25 mL). Coverslips should be placed in individual wells of a 24-well tissue culture plate. Add ~2 mL of cell suspension to each well, ensuring the coverslip is completely covered by the cell suspension. Leave the plate for 5 min at room temperature for the cells to settle and adhere to the coverslips. Adherence can be checked using a tissue culture microscope.

2.3.3 Postfixation steps for SEM: The samples are then taken through a graded series of alcohol steps in order to replace water in the cells with ethanol prior to critical point drying. It is important that the cells are not allowed to dry out. It can be helpful to have two pipettes where one is used to remove liquid and one is used to add liquid simultaneously. Remove the cell supernatant (PBS) and immediately add ~2 mL of ddH_2O. This wash step is necessary to remove any buffer salts and should be repeated once. Dehydration steps are 30%, 50%, 70%, and 90% (v/v) ethanol in H_2O added sequentially to the coverslips (at least 2 mL to each coverslip) for 5 min each, followed by 3 × 5 min in 100% ethanol. If the coverslips are not going to be taken onto the critical point dryer immediately they can be stored at 4 °C at the 70% ethanol stage. Ensure the tissue culture plate is sealed to prevent evaporation of ethanol during storage (~1 month maximum). Coverslips are ready for drying following the final 100% ethanol step. Air drying will result in deformation and collapse of the cells; to avoid these artifacts they should be dried using a critical point dryer. Carry out critical point drying according to the manufacturer's instructions. We have found that three flushes of liquid carbon dioxide, 20 min apart, with a final flush prior to drying the sample removes all the ethanol and provides a good preservation of cell shape without shrinkage.

The dried coverslips are then mounted onto SEM stubs (microscope manufacturers use different types of stubs). Silver DAG is commonly used to mount coverslips onto stubs and also acts as a conducting agent. The stubs should be left overnight to dry if using silver DAG. Alternatively, electrically conductive double-sided adhesive tape or coated carbon tabs can be used to attach the coverslip to the stubs. Finally, add a gold or platinum/palladium (80/20) coat (5–20 nm thickness or 30 s) using a sputter coater, according to the manufacturer's instructions. The stubs are now ready to be placed into an SEM.

2.3.4 Conditions for acquisition on an SEM: Trypanosomatids are relatively small cells ranging in size from ca. 5 to 50 μm (Wheeler, Gluenz, & Gull, 2013; Wheeler, Scheumann, et al., 2013). This requires particular attention to the settings of the SEM in order to produce high-quality images. There are three main settings that can influence resolution in the SEM (discounting the type of electron gun being used). The first and probably most important setting for imaging small cells is the working distance of the specimen to the objective lens. The closer the specimen is to the lens the higher the resolution using secondary electron imaging. For small cells such as these a short working distance can be critical and we typically use 5–6 mm. The second is the accelerating voltage. Resolution increases with accelerating voltage, but specimen damage and charge problems will also increase as well as noise from deeper within the sample. To obtain information from the surface only, as that is where our interest lies, we routinely use 5 kV. Finally, the lower the probe current the higher the resolution, but there are fewer secondary electrons generated, we typically use a setting between 35 and 50 when using an SEM with a normal tungsten filament gun. Particular attention should be given to the capturing conditions to obtain high-quality images. A slow (~180 s or longer, depending on sample stability) scanning/integration speed should be chosen with an image resolution between 1280 × 960 and 2560 × 1920 (or higher).

2.4 INVESTIGATING CELL CYCLE STAGES IN *T. BRUCEI* USING SEM—

Conventional SEM has proved an invaluable technique to study cell morphogenesis in *T. brucei*. Within the confines of a fixed overall shape and form, the parasite undergoes an ordered series of cell morphogenetic events that allows the cell cycle stage of individual cells to be assessed (Wheeler, Scheumann, et al., 2013). Central to this is the fact that the single flagellum remains intact during the cell division cycle. A new flagellum begins to grow alongside the old at the start of the S-phase and continues to extend throughout the remaining cell division cycle. The length of the new flagellum correlates with cell cycle stage (Woodward & Gull, 1990), so the extent of new flagellum growth can be used as an external visual marker of cell cycle progression in individual cells in asynchronous cultures (Figure 3). In all stages of the cell division cycle, except preabscission, procyclic form *T. brucei* cells can be ordered on the basis of the length of the new flagellum (Figure 3(B)–(F)). The known positioning of the new flagellum posterior to the old flagellum is a very useful marker and once the division fold has formed and there are two distinct daughter cells, it is possible to determine which is the daughter cell possessing the old flagellum and which is possessing the new flagellum due to the location of the new flagellum (Figure 3(D) and (E)). In addition, the distal tip of the new flagellum is attached to the old via a transmembrane mobile junction called the flagella connector and this connection is present in all SEM images of cells with a new flagellum (Figure 3(C) and (D), small circle). Just prior to

abscission, the two daughter cells are no longer connected at their anterior ends by the flagella connector and the cytoplasmic bridge is positioned close to the posterior ends of each daughter; this is the only point where differentiation of old and new flagella is no longer possible (Figure 3(H)).

The ability to assess cell cycle stages using SEM has also allowed a comparison to be made between the bloodstream and procyclic stages of the life cycle (Wheeler, Scheumann, et al., 2013) (Figure 3(I)–(O)). Although both life cycle forms are described as trypomastigote forms, SEM imaging of both forms has highlighted morphological differences. In the mammalian bloodstream form the flagellar pocket is located closer to the posterior end than in the procyclic form (compare Figure 3(A) and Figure 3(I)). However, there is the same morphological positioning of new flagellum located to the left of the old flagellum when viewed posterior to anterior (Figure 3(K)). A major difference between the life cycle forms is that in the bloodstream form the distal tip of the new flagellum is not attached to the old via a flagella connector. Instead the distal tip of the new flagellum lies alongside the old flagellum as it grows (Figure 3(L)). Light microscopy work established that, although the new flagellum is always positioned posterior to the old flagellum as in the procyclic form, the new flagellum does not segregate as far as in the procyclic form (Gluenz, Sharma, Carrington, & Gull, 2008). In addition, SEM demonstrated that the division fold finishes closer to the preexisting posterior end in the bloodstream form cell than in a procyclic form cell (compare Figure 3(F) with Figure 3(M)). During furrow ingression, bloodstream forms are not attached at their anterior ends as with the procyclic form (Figure 3(N)). SEM imaging also identified an additional morphological cell type in the bloodstream form called quadriflagellated cells. These cells contain four daughters that were all connected at their posterior ends, suggesting that cells had reentered the cell cycle before final abscission (Wheeler, Scheumann, et al., 2013). Morphological and morphogenetic differences in new flagellum growth are a key factor in the differences between life cycle forms and are summarized in Figure 4 (Wheeler, Scheumann, et al., 2013).

2.5 INVESTIGATING CHANGES OF CELL SHAPE AND FLAGELLUM ATTACHMENT PROPERTIES DURING DEVELOPMENT IN THE TSETSE FLY USING SEM—

During the part of their life cycle spent in the tsetse fly, *T. brucei* goes through a series of developmental changes, starting with the differentiation of the cell cycle arrested short stumpy bloodstream form to the proliferating procyclic form in the tsetse midgut. A series of historic ultrastructural studies (Vickerman, 1973; Vickerman & Luckins, 1968) and more recent (Sharma et al., 2008) studies combining electron microscopy descriptions of cellular structure with detailed morphometric measurements and analysis of fluorescently tagged reporter proteins helped to elucidate some of the important morphological changes that occur during the journey of the trypanosomes from the midgut via the proventriculus to the salivary glands (Figure 5). In the proventriculus the incoming elongated trypomastigote forms (Figure 5(A)) go through a single asymmetric division (Figure 5(B)) that produces two daughter cells with different fates (Sharma et al., 2008). The daughter cell that inherits the long old flagellum is an epimastigote form that is thought to deteriorate. The cell that inherits the newly formed flagellum, which is much shorter than the old flagellum, is a small epimastigote (Figure 5(C)), which goes on to colonize the

salivary gland. These epimastigotes eventually constitute a population of proliferating cells, with distinctive posterior end morphology, which are attached via their flagella to the tsetse salivary gland tissue (Figure 5(D)). The attached epimastigote flagella show expansion of the flagellar membrane, penetrating between host microvilli and forming punctate hemidesmosome-like attachment plaque (Tetley & Vickerman, 1985). A final differentiation event takes place in the salivary gland, which leads to the formation of the mammalian-infective metacyclic form (Figure 5(E)). This is characterized principally by reduction of mitochondrial function, acquisition of the variable surface glycoprotein coat (used for evasion of the mammalian immune response through antigenic variation), and detachment of the trypanosomes from the salivary gland tissue.

The ability to follow the fate of the old and new flagellum has been instrumental in elucidating the fates of daughter cells in differentiation divisions, such as the asymmetric division in the proventriculus (Figure 5(B)). Moreover, precise specification of new flagellum length is thought to determine the correct positioning of the division plane implying that modulation of flagellum length is an important mechanism contributing to cell fate determination (Sharma et al., 2008). Finally, there are many aspects of flagellum biology in trypanosomes that promise to reveal new insights into specific life cycle stages in the future. This includes understanding stage-specific elaborations of flagellar structures, such as the attachment plaques that mediate anchoring of epimastigotes in the tsetse salivary glands, and elucidating the role of the intertwined flagella that have been observed between postmeiotic *T. brucei* cells (putative gametes) that underwent cell fusion (Peacock, Ferris, Bailey, & Gibson, 2014).

2.6 ANALYZING FLAGELLUM LENGTH IN *L. MEXICANA* USING SEM—A detailed study of morphogenetic events in the *L. mexicana* promastigote cell cycle (Wheeler, Gluenz, & Gull, 2011) uncovered differences compared to the events described for the *T. brucei* trypomastigote forms above. Elongation of the new flagellum starts in the last third of the cell cycle and the new flagellum only emerges from the flagellar pocket at point 0.8 of the unit cell cycle, a short time before the nucleus and kinetoplast divide. For the first 80% of the cell cycle, when cells are in the G1 and S phases, the only external indicator of cell cycle progress is the progressive increase in cell body length from 5 μm to ca. 12 μm (Figure 6). During the last 20% of the cell cycle, cell length decreases rapidly, with a concomitant increase in cell width, and cytokinesis produces two short daughter cells that continue the next cycle. Unlike the situation in *T. brucei*, the length of the *L. mexicana* flagellum is not directly correlated with position in the cell cycle: the new flagellum grows to a length of 4–5 μm during its first cycle but then continues to grow in length over the next cell cycles. As a consequence the length of the old flagellum on dividing cells is heterogeneous, ranging from ca. 5 μm to nearly 20 μm. Except for the length of the new flagellum during a very short time at the end of the cell cycle, flagellum length does not provide a useful marker of a cell's progress through the cell cycle (Figure 6(E)).

In the mammalian host, *L. mexicana* parasites invade host phagocytes (neutrophils, dendritic cells, and their principal host cell, the macrophage). On entry into a phagocyte, promastigotes, with their long highly motile flagellum (Figure 7(A)), transform into small round amastigotes (Figure 7(B)), which are adapted to survive in the harsh conditions of a

phagolysosome. The distal tip of the amastigote flagellum, which is difficult to see by light microscopy, can be seen in scanning electron micrographs to protrude a short distance from the flagellar pocket into the external milieu (Figure 7(B)). Thin-section TEM and electron tomography were used to show that this change in length was accompanied by a change in axoneme structure: the promastigote flagellum has a canonical 9 + 2 axoneme structure (Figure 7(C) and (D)) while the amastigote flagellum has in its distal segment a collapsed bundle of 9 outer doublet microtubules (9v axoneme), lacking the central pair apparatus and dynein arms (Figure 7(E)) (Gluenz et al., 2010).

2.7 THREE-DIMENSIONAL EM METHODS TO STUDY THE FLAGELLUM IN *T. BRUCEI* AND *LEISHMANIA* SPP.: TOMOGRAPHY

2.7.1 Cellular electron tomography: There are a range of three-dimensional electron microscopy techniques to study the internal ultrastructure of cells. Cellular electron tomography is a powerful tool using transmission electron microscopes to obtain high-resolution three-dimensional views of individual organelles and structures within cells and tissues. In dual-axis tomography a thick section of sample, typically 200–300 nm, is used. The sample is tilted, typically −70° to +70°, and images are recorded every 1°–2°. Dual-axis datasets are achieved by rotating the grid by 90° and taking the second tilt series at the same location on the sample. There are various software packages (commercial and freely available) that automate the collection of single- and dual-axis datasets but the data can also be collected manually. The resulting image stack is then aligned and combined to generate three-dimensional tomograms using a back-projection algorithm; we use eTomo (IMOD, Boulder, CO, USA), but there are several other software programs that can achieve the same result. An in-depth discussion of the various fixation techniques and considerations for tomography are outside the scope of this chapter and have been covered extensively in McIntosh (2007). This technique has been invaluable for three-dimensional reconstructions of the flagellar pocket (Lacomble et al., 2009), illustrating the spatial organization of basal body movements within the flagellar pocket region (Lacomble et al., 2010), ultrastructure of the PFR (Hughes et al., 2012), spatial organization of the endoplasmic reticulum surrounding the four rootlet microtubules (MtQ) (Lacomble et al., 2012), and the ultrastructural organization at the distal tip of the growing flagellum (Hoog et al., 2013; Hughes, Towers, Starborg, Gull, & Vaughan, 2013).

2.7.2 Primary fixation for tomography: There are a variety of methods for preparing cells for cellular electron tomography. We have used chemical fixation as per protocol for SBFSEM below (Section 3.8). High-pressure freezing of samples is also commonly used for tomography (Weise, Stierhof, Kuhn, Wiese, & Overath, 2000) and the protocol for preparing samples for *T. brucei* is outlined in Hoog, Gluenz, Vaughan, and Gull (2010). Whichever primary fixation method is used, the sample is embedded in resin to produce a block containing a pellet of fixed cells. Cryo electron tomography can also be used on isolated organelles that have been plunge frozen and this technique has been applied to studies of the flagellum in *T. brucei* (Hoog et al., 2012; Hughes et al., 2012).

2.7.3 Sectioning and staining blocks for tomography: Formvar-coated copper slot grids should be used for collecting dual-axis tomograms to ensure that grid bars do not hinder

collection of the tilt series. A method for collecting serial sections using a diamond knife is outlined in Hoog et al. (2010). The thickness of sections for tomography is generally limited by the kV of the microscope. If the section is too thick then electrons will not pass through the sample and the resolution will be low. We found that 120–200 nm sections were suitable for our purposes on a 120 kV microscope. Sections are stained using a triple-staining method described below to increase contrast and reduce staining precipitates (Hayat, 2000). It is important to use fresh stains, to filter them immediately prior to use, and only use lead citrate at pH 12. We apply the grids (section side down so that it is in contact with the stain) to small drops of each stain on a clean sheet of Parafilm, inside a glass Petri dish with NaOH pellets around the edges. The grids are suspended on each droplet as follows, ddH_2O (1 min), 2% aqueous uranyl acetate (6–8 min), three drops of ddH_2O (1 min each), Reynold's lead citrate (8 min), two drops of 0.1 N NaOH (quick rinses with solution wicked away from the grids immediately), three drops of ddH_2O (1 min each), 2% aqueous uranyl acetate (5–8 min), and a final rinse in three drops of ddH_2O. Ten nanometer gold fiducials are added to each side of the sample by suspending the grid onto a droplet of unconjugated 10 nm undiluted colloidal gold (British Biocell International) for 30 s, blotting, and placing the opposite side of the grid onto the droplet for a further 30 s. The grid is then blotted and left to dry for a few minutes before being placed in the microscope.

2.7.4 Three-dimensional microscopy of the flagellar pocket: The single flagellum exits the cell body via invagination of the cell membrane called the flagellar pocket in *T. brucei*, which is the only site for endocytosis and exocytosis in the cell (Field & Carrington, 2004). The flagellar pocket is critical for trafficking and recycling of glycosylphosphatidylinositol-anchored proteins on the cell surface which are required for antigenic variation and survival in the host organism (Borst & Cross, 1982) and plays a key role in cellular morphogenesis during cell division (Absalon et al., 2008; Lacomble et al., 2010). The equivalent of a flagellar pocket has been identified in some mammalian cell types—called the ciliary pocket (for review see Ghossoub, Molla-Herman, Bastin, & Benmerah, 2011).

For dual-axis cellular electron tomography of chemically fixed whole trypanosome cells, serial tomograms from 250-nm-thick sections were required to encompass the region of the flagellar pocket (~2 mm^3). The ability to view this complex cellular structure in three dimensions has been critical to our understanding of the spatial organization of the pocket and the position of many cytoskeleton structures and organelles immediately surrounding the pocket (Lacomble et al., 2009) (Figure 8(A) and (B)). A method has been developed to orientate tomograms so that tomograms can be compared during cell division (Figure 8(C) and (D)). The center of the proximal end of the basal body is the origin point, the *z*-axis runs up the axoneme from proximal toward distal with the central pair microtubules orientated along the *x*-axis and the *y*-axis pointing toward the probasal body. Development of these coordinates then allowed flagellar pocket tomograms to be compared. This has enabled a dissection of flagellar pocket duplication and segregation during the cell division cycle (Figure 8(E)–(G)). This demonstrated that the new flagellum performs an anticlockwise rotation around the old flagellum within the flagellar pocket prior to segregation of the pocket. Compare Figure 8(E3) where the probasal body is in quadrant 2, with Figure 8(F3) where the probasal body has matured and a new flagellum has invaded the existing flagellar

pocket and is still situated in quadrant 2 and finally Figure 8(G3) where the new flagellum is now located in quadrant 4 (Lacomble et al., 2010).

2.8 THREE-DIMENSIONAL EM METHODS: SERIAL BLOCK FACE SCANNING ELECTRON MICROSCOPY—Serial block face scanning electron microscopy (SBFSEM) is a relatively new technique and involves collecting hundreds of sequential serial sections producing three-dimensional views of individual cells and large areas of tissue. The ultrastructure of cells and tissues is traditionally studied using a TEM. However, the drawback of this technique is the need for very thin slices of cells or tissues (~70–100 nm), which limits the area that can be visualized. It is possible to collect multiple serial sections and image them in order to build a three-dimensional model of a volume; however, this is technically challenging and for the majority of users is only possible for small areas of the cell or tissue. Denk and Horstmann (2004) developed SBFSEM in which an ultramicrotome is mounted into the chamber of a field emission scanning electron microscope. Using a backscatter detector mounted in an SEM it is possible to obtain similar images to that obtained by a conventional TEM (Figure 9(A)). This is due to the fact that both techniques use electron scattering to produce an image. Heavy elements scatter electrons more strongly than light elements, creating a shadow in the projected TEM image and a bright backscattered electron signal in the SEM.

To image cells by SBFSEM, a trimmed resin block containing either a cell pellet or block of tissue is mounted onto the specimen stage. A section of the block face is cut (usually 25–200 nm) and the block face is imaged. The block face advances a set amount (usually 25–200 nm) and is cut by the diamond knife of the ultramicrotome. The block face is then imaged and then advances a set amount and cut again by the diamond knife. This results in an automated collection of serial sections, which can be in the hundreds or thousands and require little or no cross correlation following image capture (Hughes, Hawes, Monteith, & Vaughan, 2014).

2.8.1 Important considerations in the preparation of cells for SBFSEM: There are two important considerations when preparing samples for SBFSEM studies. The first is the requirement for contrast in the sample. Heavy metals such as osmium tetroxide and uranyl acetate have been widely used during sample preparation for TEM. In conventional TEM addition of further heavy metals occurs “on section” by poststaining sections mounted on TEM grids with uranyl acetate and lead citrate. However, “on section” heavy metal staining is not possible with SBFSEM; therefore, contrast has to be achieved during the fixation procedure. The second important consideration in preparing cells for SBFSEM is the problem of buildup of electrostatic charge on the surface of the block face. In traditional SEM, samples such as biological specimens, which are not electrically conductive, are grounded by the addition of a fine coating of gold, platinum/palladium, carbon, or other conductive material. In SBFSEM the diamond knife exposes uncoated resin (the sample block can be coated as normal prior to putting it into the chamber), which can be prone to charging. The addition of heavy metals in the fixation not only provides much needed contrast, but also aids in reducing the buildup of electrostatic charge. In cell pellets such as those for *T. brucei* and *L. mexicana* there is inevitably empty resin between cells and this

can cause problems when imaging in a high vacuum environment. Many SBFSEM microscopes are designed with a variable pressure specimen chamber, essential for specimens with relatively large areas of resin between cells. The buildup of charge can be balanced by varying the chamber pressure with a tradeoff in the final resolution that can be obtained. However, this technology is improving constantly and resolution limits are increasing.

2.8.2 Primary fixation of cells from a suspension culture: A 25 mL culture of procyclic form trypanosomes or promastigote form *L. mexicana* grown to ~5×10^6 cells/mL will yield two good-sized pellets suitable for SBFSEM. Bloodstream form trypanosomes are grown at a lower density and are routinely harvested at ~8×10^5 cells/mL and 50 mL culture will only provide two good-sized pellets for SBFSEM. Fixation should ideally be carried out in the suspension culture in order to minimize manipulation of cells prior to fixation. The initial fixation steps are the same as previously described for TEM sample preparation in Hoog et al. (2010). The most important parts of this will be repeated here to aid the reader. EM-grade glutaraldehyde should be added directly to the suspension culture directly from the incubator to a final concentration of 2.5% glutaraldehyde (from a 25% stock of EM-grade glutaraldehyde). Cells are incubated for 5 min at room temperature and harvested by moving the suspension to a 50 mL falcon tube (depending on the volume of cells) and centrifuged (800 g) for 10 min. Supernatant is removed and the cell pellet is resuspended in 1 mL of buffered fixative (2.5% glutaraldehyde, 2% fresh paraformaldehyde in 100 mM phosphate buffer pH 7.0). The sample should be moved to a 1.5–2 mL Eppendorf tube for the remainder of the fixation for ease of manipulation. The cells should be centrifuged again in the Eppendorf tube (800 g) to form a pellet. The aim is to keep the cells in this pellet for the remainder of the processing as it avoids loss of cells in the subsequent steps. The pellet should be left for at least 2 h at room temperature. Samples may be left at 4 °C overnight or longer periods if necessary. At this stage samples can be transported if required.

2.8.3 Postfixation, dehydration, and resin embedding: Postfixation is where heavy metals are added to the sample. The method outlined here has been successful for SBFSEM samples of *T. brucei*. Samples are postfixed in 1% osmium (in 100 mM phosphate buffer) for 1 h at room temperature and the pellet will go a dark brown. Osmium tetroxide acts as both a fixative and a stain, reacting with lipids, oxidizing unsaturated bonds of fatty acids, and also increasing contrast in the sample. Following osmium fixation any phosphate ions must be removed by at least three washes in distilled water. This prevents precipitation of uranyl acetate in the subsequent step. Uranyl acetate is also used in the postfixation step to add further contrast to the samples, traditionally called en bloc staining. Two percent magnesium uranyl acetate in water is added to the cell pellet and left overnight at 4 °C. Samples should be kept in the dark as uranyl acetate will precipitate when exposed to light.

Following en bloc staining, the water must be removed as it is not miscible with most resins. Dehydration is performed by gradually increasing the concentration of a solvent, usually ethanol or acetone. Dehydration is performed in a series of washes with increasing concentration of dehydrated acetone: the pellets are immersed in 30%, 50%, 70%, 90% (v/v) acetone in water for 15 min each and three times 100% dehydrated acetone for 30 min each.

The pellet is then ready for resin infiltration. A hard resin should be used for embedding samples for SBFSEM as the resin is sensitive to beam damage. This is especially important when cutting thin sections as the damage can penetrate to a depth greater than the next section. The hard Agar 100 epoxy resin has been successful in our studies. Infiltration begins by immersing the pellets in a mixture of three parts acetone to one part resin (3:1) for 3 h, followed by a 1:1 acetone to resin mixture for 3 h and then a 1:3 acetone to resin mix for 3 h. The pellet should be left in 100% resin overnight at room temperature. The next day, two further changes in 100% resin for 3 h each are required. It is important to consider the holder for the cell pellet when it is polymerized, as cubes of sample need to be cut from the resin blocks afterwards—see below. We either use Eppendorf tubes or move to flat-bottomed BEEM capsules. The pellets are polymerized for 24 h at 70 °C.

2.8.4 Preparation of blocks for SBFSEM and settings on the microscope: A Quanta 250 FEG (FEI, Eindhoven, Netherlands) with a fitted Gatan 3view system (Gatan, Abingdon, Oxfordshire, UK) was used in our current studies. A cube ~2–2.5 mm^3 of sample is required to mount on a 3view stub. This is achieved by holding the resin block in a vice and making multiple cuts with a hack saw. The block is then rotated 90° and multiple cuts applied again, producing small cubes that can be trimmed and mounted. The sample is attached to the stub using conductive superglue and left overnight to dry. The cube is then trimmed to produce a long thin trapezium shape (similar in principle to the trimming of a block face for thin-section TEM) ready for cutting on SBFSEM. Finally, the stub is sputter coated with gold to aid in conductivity around the block face. As already mentioned, the settings on SBFSEM are sample dependent. Conditions used for collecting samples for SBFSEM imaging of the distal tip of the new flagellum in *T. brucei* bloodstream forms (Hughes et al., 2013) are given as an example. Serial images of the block face were recorded at an accelerating voltage of 5 kV, a spot size of 2.5, and a pressure of 0.5 Torr. The pixel dwell time was 5 μs, pixel size was 6–6.2 nm, and slice thickness was 100 nm.

2.8.5 Data processing and segmentation of SBFSEM images: Images are recorded using Digital Micrograph on the 3view system. Output is a series of digital micrograph files that can be converted and combined into an.mrc file format using the free IMOD software (Kremer, Mastronarde, & McIntosh, 1996) creating a single movie file of all the slices. No image alignment is usually required, but if there is a minor issue of correlation between two slices, it can be corrected using the MIDAS function on IMOD software. Individual whole cells or portions of an individual cell are manually selected in IMOD by following slices of individual cells through the dataset. The area of interest is then boxed out using the trimvol function of IMOD and a volume of the desired area is produced. There are now a number of software packages available to produce a three-dimensional model (called segmentation) of the desired area from slices obtained from SBFSEM volume datasets (Figure 9(B) and (C)). In our studies we have used Amira where distinct characteristics such as organelles and plasma membrane can be modeled using a combination of automatic thresholding, interpolation, and manual “brush” tools. Access to computing and storage should not be overlooked and requirements are available from the microscope manufacturers. Individual datasets can produce ~15–20 GB of data in a 24-h period and a good-sized server of ~10 TB minimum is recommended for data storage.

2.9 COMBINING THREE-DIMENSIONAL MICROSCOPY METHODS FOR THE STUDY OF THE DISTAL TIP OF THE NEW FLAGELLUM OF *T. BRUCEI* BLOODSTREAM FORMS—

SEM of procyclic form cells revealed that the distal tip of the growing new flagellum was attached to the old flagellum via the flagella connector (Briggs et al., 2004; Moreira-Leite, Sherwin, Kohl, & Gull, 2001) (Figures 1(B) and 3). As the old flagellum can be distinguished from the new in thin-section TEM cross sections this allows identification of the distal tip of the new flagellum in random and serial thin sections. The flagella connector is proposed to act as a guide for growth of the new flagellum in a process known as cytotaxis (Moreira-Leite et al., 2001). However, this intriguing structure was not identified at the distal tip of the bloodstream form of the parasite (Briggs et al., 2004).

The bloodstream form cells exhibit the same morphogenetic cues as the procyclic form, allowing the new flagellum to be distinguished from the old flagellum. We were thus able to investigate the structure of the bloodstream form's new flagellum tip using a combination of cellular electron tomography and SBFSEM. Four serial dual-axis tomograms were required to incorporate the full three-dimensional view of the area of the distal tip of the new flagellum and it was found to be located in a deep indentation of the cell body membrane structure called the groove (Hughes et al., 2013) (Figure 10(A)). In order to discover if the groove was present during the entire growth phase of the new flagellum SBFSEM was used to produce serial sections of individual trypanosomes. This combination approach enables the high-resolution details of the ultrastructure of an organelle or cellular structure to be investigated by cellular electron tomography, but it can then be put into the context of a whole individual cell. SBFSEM datasets containing 1000 adjacent sections 100 nm thick were collected of an asynchronous bloodstream form culture, giving large numbers of serial sections through entire individual cells at various stages of the cell division cycle. This combination approach demonstrated that the groove was observed during the growth phase of the new flagellum (Figure 10(B) and (C)) (Hughes et al., 2013). The resolution of SBFSEM images used in this study does not permit the visualization of individual components of the groove as described in tomograms; instead the indentation of the cell body membrane and the increased electron density of the groove area can be used for identification (Figure 10(C)). This combination approach of integrating tomography with SBFSEM is a powerful new method to interrogate many other aspects of flagellum biology.

3. MATERIALS

3.1 CELLS, MEDIA, AND BUFFERS—

SDM-79 and HMI-9 media are manufactured by Life Technologies to custom specifications. References in the main text detail the composition of these media.

Medium M199 powder (Life Technologies)

Schneider's *Drosophila* medium (Life Technologies)

Fetal bovine serum, heat inactivated, South American Origin (Life Technologies, catalogue number 10500-064): suitable for growth of *L. mexicana*

Hemin (Sigma Aldrich Company Ltd, Gillingham, UK)

4-(2-Hydroxyethyl)piperazine-1-ethanesulfonic acid (HEPES; Sigma Aldrich Company Ltd, Gillingham, UK)

4-Morpholineethanesulfonic acid sodium salt (MES; Sigma Aldrich Company Ltd, Gillingham, UK)

PEME (100 mM 1,4-piperazinediethanesulfonic acid (PIPES), 2 mM ethylene glycol-bis(2-aminoethylether)-*N,N,N′,N′*-tetraacetic acid (EGTA), 1 mM

$MgSO_4$, 0.1 mM (ethylenediaminetetraacetic acid) EDTA, pH 6.9; chemicals from Sigma Aldrich Company Ltd, Gillingham, UK)

Phosphate-buffered saline (PBS) tablets (Sigma Aldrich Company Ltd, Gillingham, UK)

3.2 CHEMICALS AND REAGENTS—Paraformaldehyde (Sigma Aldrich Company Ltd, Gillingham, UK)

Glutaraldehyde EM grade (TAAB, UK)

Uranyl acetate (Amsbio, Abingdon, UK)

Lead citrate (TAAB, UK)

Dehydrated methanol (Sigma Aldrich Company Ltd, Gillingham, UK)

Dehydrated acetone (Science Services GmbH, Berlin, Germany)

Osmium tetroxide (Amsbio, Abingdon, UK)

Poly-L-lysine (Sigma Aldrich Company Ltd, Gillingham, UK)

3.3 RESINS AND EM CONSUMABLES—Agar 100 Resin Hard (Agar Scientific, Stansted, UK)

Silver DAG (TAAB, UK)

Conductive adhesive tape (Agar Scientific, Stansted, UK)

13 mm glass coverslips (VWR International, PA, USA)

Thermanox coverslips (Agar Scientific, Stansted, UK)

Costar 24-well cell culture plates (Thermo Fisher Scientific)

Conductive superglue (Agar Scientific/TAAB).

Gold fiducial markers/10 nm colloidal gold (British Biocell International)

3.4 SOFTWARE—DigitalMicrograph™ (Gatan Inc., Abingdon, UK)

Amira® (FEI, Eindhoven, Netherlands)

IMOD (University of Boulder, CO, USA)

4. DISCUSSION

In this chapter we have described methods for studying flagellum growth and structure in trypanosomatids. The importance of the flagellum in directing correct formation of a new daughter cell and the known and suspected roles in pathogenicity have made this organelle an important focus for detailed structural studies. It was clear from earlier morphological studies using light microscopy and conventional TEM that there was precise spatial positioning of organelles and cellular structures within cells. SEM has been invaluable in describing the external morphogenetic patterning in these cells and the role of the *T. brucei* flagellum in directing correct formation of a new daughter cell. The ability to order *T. brucei* cells according to the length of the new flagellum has aided in the identification of previously unknown morphological cell cycle types.

SEM has also highlighted the change in the length of the flagellum during differentiation in the life cycle of these parasites and at least in the differentiation events so far studied the daughter cell inheriting the new flagellum is the cell that continues with life cycle, but the fate of the old flagellum daughter is not entirely understood. Further work elucidating expression profiles of flagellum genes during differentiation could yield a greater understanding of the control of flagellum growth. In addition, the flagellum is also required for parasite attachment in the insect vector which is essential for pathogenicity and a comparison of gene expression profiles between attached and unattached forms could aid in the identification of novel genes involved in this process.

Investigating the internal cellular architecture at an ultrastructural level in a spatial context has always been challenging. Cellular electron tomography has allowed unprecedented understanding of the spatial architecture of the flagellum and growth of a new flagellum at the distal tip in *T. brucei* and the changes to flagellum structure in *L. mexicana*. The major drawback is that dual-axis tomography is relatively time-consuming to produce and reconstruct, making large-scale quantitative analysis unrealistic. The modeling (segmentation) of data is the most time-consuming aspect of this technique, but future developments in automated modeling software may reduce processing time. Integration of SBFSEM with cellular electron tomography offers opportunities to study individual cellular structures at high resolution using cellular electron tomography within the context of whole individual cells or parasite cells inside host cells. Datasets containing hundreds of individual cells are relatively straightforward to produce allowing mutant phenotypes to be dissected in a whole-cell context for the first time.

The protocols and investigative strategies detailed in this chapter are based on our research specifically on *T. brucei* and *L. mexicana*, with a focus on cell morphogenesis, flagellar assembly, and modulation of axoneme structure. With minor modifications these protocols and methods will be applicable to the investigation of other kinetoplastid species. These unicellular eukaryotes have proven excellent model organisms for studying lineage-specific and universally conserved biology of eukaryotic cilia and flagella.

Europe PMC Funders Author Manuscripts

ACKNOWLEDGMENTS

Some of the methods and studies described in this chapter were conceived and developed in the laboratory of Professor Keith Gull (University of Oxford) whom we would like to thank for helpful discussions and support. We would also like to thank Dr Mike Shaw and Dr Errin Johnson (University of Oxford) and Mr Tobias Starborg for assistance with protocol development. EG is a Royal Society University Research Fellow. RW is a Wellcome Trust Sir Henry Wellcome Postdoctoral Fellow. Work in SV's lab is funded by the BBSRC.

REFERENCES

Absalon S, Blisnick T, Bonhivers M, Kohl L, Cayet N, Toutirais G, et al. Flagellum elongation is required for correct structure, orientation and function of the flagellar pocket in *Trypanosoma brucei*. Journal of Cell Science. 2008; 121:3704–3716. [PubMed: 18940910]

Akiyoshi B, Gull K. Evolutionary cell biology of chromosome segregation: insights from trypanosomes. Open Biology. 2013; 3:130023. [PubMed: 23635522]

Bastin P, Sherwin T, Gull K. Paraflagellar rod is vital for trypanosome motility. Nature. 1998; 391:548. [PubMed: 9468133]

Bates PA. Complete developmental cycle of *Leishmania mexicana* in axenic culture. Parasitology. 1994; 108(Pt 1):1–9. [PubMed: 8152848]

Bates PA. Transmission of *Leishmania metacyclic* promastigotes by phlebotomine sand flies. International Journal for Parasitology. 2007; 37:1097–1106. [PubMed: 17517415]

Borst P, Cross GA. Molecular basis for trypanosome antigenic variation. Cell. 1982; 29:291–303. [PubMed: 6811137]

Briggs LJ, McKean PG, Baines A, Moreira-Leite F, Davidge J, Vaughan S, et al. The flagella connector of *Trypanosoma brucei*: an unusual mobile transmembrane junction. Journal of Cell Science. 2004; 117:1641–1651. [PubMed: 15075226]

Brun R, Schonenberger. Cultivation and in vitro cloning or procyclic culture forms of *Trypanosoma brucei* in a semi-defined medium. Acta Tropica. 1979; 36:289–292. [PubMed: 43092]

van Dam TJ, Townsend MJ, Turk M, Schlessinger A, Sali A, Field MC, et al. Evolution of modular intraflagellar transport from a coatomer-like progenitor. Proceedings of the National Academy of Sciences USA. 2013; 110:6943–6948.

Denk W, Horstmann H. Serial block-face scanning electron microscopy to reconstruct three-dimensional tissue nanostructure. PLoS Biology. 2004; 2:e329. [PubMed: 15514700]

Deschamps P, Lara E, Marande W, Lopez-Garcia P, Ekelund F, Moreira D. Phylogenomic analysis of kinetoplastids supports that trypanosomatids arose from within bodonids. Molecular Biology and Evolution. 2011; 28:53–58. [PubMed: 21030427]

Engstler M, Pfohl T, Herminghaus S, Boshart M, Wiegertjes G, Heddergott N, et al. Hydrodynamic flow-mediated protein sorting on the cell surface of trypanosomes. Cell. 2007; 131:505–515. [PubMed: 17981118]

Field MC, Carrington M. Intracellular membrane transport systems in *Trypanosoma brucei*. Traffic (Copenhagen, Denmark). 2004; 5:905–913.

Gadelha AP, Cunha-e-Silva NL, de Souza W. Assembly of the *Leishmania amazonensis* flagellum during cell differentiation. Journal of Structural Biology. 2013; 184:280–292. [PubMed: 24041804]

Ghossoub R, Molla-Herman A, Bastin P, Benmerah A. The ciliary pocket: a once-forgotten membrane domain at the base of cilia. Biology of the Cell. 2011; 103:131–144. [PubMed: 21275905]

Gluenz E, Ginger ML, McKean PG. Flagellum assembly and function during the Leishmania life cycle. Current Opinion in Microbiology. 2010; 13:473–479. [PubMed: 20541962]

Gluenz E, Hoog JL, Smith AE, Dawe HR, Shaw MK, Gull K. Beyond 9 + 0: noncanonical axoneme structures characterize sensory cilia from protists to humans. FASEB Journal: Official Publication of the Federation of American Societies for Experimental Biology. 2010; 24:3117–3121. [PubMed: 20371625]

Gluenz E, Sharma R, Carrington M, Gull K. Functional characterization of cohesin subunit SCC1 in *Trypanosoma brucei* and dissection of mutant phenotypes in two life cycle stages. Molecular Microbiology. 2008; 69:666–680. [PubMed: 18554326]

Gossage SM, Rogers ME, Bates PA. Two separate growth phases during the development of Leishmania in sand flies: implications for understanding the life cycle. International Journal for Parasitology. 2003; 33:1027–1034. [PubMed: 13129524]

Gull K. The cytoskeleton of trypanosomatid parasites. Annual Review of Microbiology. 1999; 53:629–655.

Hayat, M. Principles and techniques of electron microscopy, biological applications. Cambridge University Press; Cambridge: 2000.

Hemphill A, Lawson D, Seebeck T. The cytoskeletal architecture of *Trypanosoma brucei*. Journal of Parasitology. 1991; 77:603–612. [PubMed: 1865269]

Hill KL. Biology and mechanism of trypanosome cell motility. Eukaryotic Cell. 2003; 2:200–208. [PubMed: 12684369]

Hirumi H, Hirumi K. Axenic culture of African trypanosome bloodstream forms. Parasitology Today. 1994; 10:80–84. [PubMed: 15275508]

Hoare CA, Wallace FG. Developmental stages of trypanosomatid flagellates: a new terminology. Nature. 1966; 212:1385–1386.

Hoog JL, Bouchet-Marquis C, McIntosh JR, Hoenger A, Gull K. Cryo-electron tomography and 3-D analysis of the intact flagellum in *Trypanosoma brucei*. Journal of Structural Biology. 2012; 178:189–198. [PubMed: 22285651]

Hoog JL, Gluenz E, Vaughan S, Gull K. Ultrastructural investigation methods for *Trypanosoma brucei*. Methods in Cell Biology. 2010; 96:175–196. [PubMed: 20869523]

Hoog JL, Lacomble S, O'Toole ET, Hoenger A, McIntosh JR, Gull K. Modes of flagellar assembly in Chlamydomonas reinhardtii and *Trypanosoma brucei*. eLife. 2013; 3:e01479. [PubMed: 24448408]

Hoog JL, Lacomble S, O'Toole ET, Hoenger A, McIntosh JR, Gull K. Modes of flagellar assembly in Chlamydomonas reinhardtii and *Trypanosoma brucei*. eLife. 2014; 3:e01479. [PubMed: 24448408]

Hughes L, Hawes C, Monteith S, Vaughan S. Serial block face scanning electron microscopy–the future of cell ultrastructure imaging. Protoplasma. 2014; 251:395–401. [PubMed: 24240569]

Hughes LC, Ralston KS, Hill KL, Zhou ZH. Three-dimensional structure of the Trypanosome flagellum suggests that the paraflagellar rod functions as a biomechanical spring. PLoS One. 2012; 7:e25700. [PubMed: 22235240]

Hughes L, Towers K, Starborg T, Gull K, Vaughan S. A cell-body groove housing the new flagellum tip suggests an adaptation of cellular morphogenesis for parasitism in the bloodstream form of *Trypanosoma brucei*. Journal of Cell Science. 2013; 126:5748–5757. [PubMed: 24127564]

Killick-Kendrick R, Molyneux DH, Ashford RW. Leishmania in phlebotomid sandflies. I. Modifications of the flagellum associated with attachment to the mid-gut and oesophageal valve of the sandfly. Proceedings of the Royal Society of London. Series B, Containing Papers of a Biological Character. Royal Society. 1974; 187:409–419.

Kohl L, Sherwin T, Gull K. Assembly of the paraflagellar rod and the flagellum attachment zone complex during the *Trypanosoma brucei* cell cycle. Journal of Eukaryotic Microbiology. 1999; 46:105–109. [PubMed: 10361731]

Kremer JR, Mastronarde DN, McIntosh JR. Computer visualization of three-dimensional image data using IMOD. Journal of Structural Biology. 1996; 116:71–76. [PubMed: 8742726]

Lacomble S, Vaughan S, Deghelt M, Moreira-Leite FF, Gull K. A *Trypanosoma brucei* protein required for maintenance of the flagellum attachment zone and flagellar pocket ER domains. Protist. 2012; 163:602–615. [PubMed: 22186015]

Lacomble S, Vaughan S, Gadelha C, Morphew MK, Shaw MK, McIntosh JR, et al. Three-dimensional cellular architecture of the flagellar pocket and associated cytoskeleton in trypanosomes revealed by electron microscope tomography. Journal of Cell Science. 2009; 122:1081–1090. [PubMed: 19299460]

Lacomble S, Vaughan S, Gadelha C, Morphew MK, Shaw MK, McIntosh JR, et al. Basal body movements orchestrate membrane organelle division and cell morphogenesis in *Trypanosoma brucei*. Journal of Cell Science. 2010; 123:2884–2891. [PubMed: 20682637]

Lukes J, Hashimi H, Zikova A. Unexplained complexity of the mitochondrial genome and transcriptome in kinetoplastid flagellates. Current Genetics. 2005; 48:277–299. [PubMed: 16215758]

Matthews KR. The developmental cell biology of *Trypanosoma brucei*. Journal of Cell Science. 2005; 118:283–290. [PubMed: 15654017]

McIntosh JR. Cellular electron microscopy. Methods in Cell Biology. 2007; 79:1–850.

McKean PG, Baines A, Vaughan S, Gull K. Gamma-tubulin functions in the nucleation of a discrete subset of microtubules in the eukaryotic flagellum. Current Biology. 2003; 13:598–602. [PubMed: 12676092]

Molla-Herman A, Ghossoub R, Blisnick T, Meunier A, Serres C, Silbermann F, et al. The ciliary pocket: an endocytic membrane domain at the base of primary and motile cilia. Journal of Cell Science. 2010; 123:1785–1795. [PubMed: 20427320]

Moreira-Leite FF, Sherwin T, Kohl L, Gull K. A trypanosome structure involved in transmitting cytoplasmic information during cell division. Science. 2001; 294:610–612. [PubMed: 11641501]

Morga B, Bastin P. Getting to the heart of intraflagellar transport using Trypanosoma and Chlamydomonas models: the strength is in their differences. Cilia. 2013; 2:16. [PubMed: 24289478]

Peacock L, Ferris V, Bailey M, Gibson W. Mating compatibility in the parasitic protist *Trypanosoma brucei*. Parasites and Vectors. 2014; 7:78. [PubMed: 24559099]

Ralston KS, Kabututu ZP, Melehani JH, Oberholzer M, Hill KL. The *Trypanosoma brucei* flagellum: moving parasites in new directions. Annual Review of Microbiology. 2009; 63:335–362.

Robinson DR, Gull K. Basal body movements as a mechanism for mitochondrial genome segregation in the trypanosome cell cycle. Nature. 1991; 352:731–733. [PubMed: 1876188]

Robinson DR, Sherwin T, Ploubidou A, Byard EH, Gull K. Microtubule polarity and dynamics in the control of organelle positioning, segregation, and cytokinesis in the trypanosome cell cycle. Journal of Cell Biology. 1995; 128:1163–1172. [PubMed: 7896879]

Rogers ME, Chance ML, Bates PA. The role of promastigote secretory gel in the origin and transmission of the infective stage of *Leishmania mexicana* by the sandfly *Lutzomyia longipalpis*. Parasitology. 2002; 124:495–507. [PubMed: 12049412]

Rogers ME, Ilg T, Nikolaev AV, Ferguson MA, Bates PA. Transmission of cutaneous leishmaniasis by sand flies is enhanced by regurgitation of fPPG. Nature. 2004; 430:463–467. [PubMed: 15269771]

Rotureau B, Ooi CP, Huet D, Perrot S, Bastin P. Forward motility is essential for trypanosome infection in the tsetse fly. Cellular Microbiology. 2014; 16:425–433. [PubMed: 24134537]

Sharma R, Peacock L, Gluenz E, Gull K, Gibson W, Carrington M. Asymmetric cell division as a route to reduction in cell length and change in cell morphology in trypanosomes. Protist. 2008; 159:137–151. [PubMed: 17931969]

Sherwin T, Gull K. The cell division cycle of *Trypanosoma brucei brucei*: timing of event markers and cytoskeletal modulations. Philosophical Transactions of the Royal Society London B: Biological Sciences. 1989; 323:573–588.

Stuart K, Brun R, Croft S, Fairlamb A, Gurtler RE, McKerrow J, et al. Kinetoplastids: related protozoan pathogens, different diseases. The Journal of Clinical Investigation. 2008; 118:1301–1310. [PubMed: 18382742]

Tetley L, Vickerman K. Differentiation in *Trypanosoma brucei*: host-parasite cell junctions and their persistence during acquisition of the variable antigen coat. Journal of Cell Science. 1985; 74:1–19. [PubMed: 4030903]

Vaughan S, Shaw M, Gull K. A post-assembly structural modification to the lumen of flagellar microtubule doublets. Current Biology. 2006; 16:R449–R450. [PubMed: 16781996]

Vickerman K. The fine structure of *Trypanosoma congolense* in its bloodstream phase. Journal of Protozoology. 1969a; 16:54–69. [PubMed: 4896668]

Vickerman K. On the surface coat and flagellar adhesion in trypanosomes. Journal of Cell Science. 1969b; 5:163–193. [PubMed: 5353653]

Vickerman K. The mode of attachment of *Trypanosoma vivax* in the proboscis of the tsetse fly *Glossina fuscipes*: an ultrastructural study of the epimastigote stage of the trypanosome. Journal of Protozoology. 1973; 20:394–404. [PubMed: 4731343]

Vickerman K. Developmental cycles and biology of pathogenic trypanosomes. British Medical Bulletin. 1985; 41:105–114. [PubMed: 3928017]

Vickerman K, Luckins AG. Cyclical transformation in trypanosomes. Journal of General Microbiology. 1968; 50(Suppl.):12–13. [PubMed: 5652079]

Vickerman K, Tetley L, Hendry KA, Turner CM. Biology of African trypanosomes in the tsetse fly. Biology of the Cell. 1988; 64:109–119. [PubMed: 3067793]

Weise F, Stierhof YD, Kuhn C, Wiese M, Overath P. Distribution of GPI-anchored proteins in the protozoan parasite Leishmania, based on an improved ultrastructural description using high-pressure frozen cells. Journal of Cell Science. 2000; 113(Pt 24):4587–4603. [PubMed: 11082051]

Wheeler RJ, Gluenz E, Gull K. The cell cycle of Leishmania: morphogenetic events and their implications for parasite biology. Molecular Microbiology. 2011; 79:647–662. [PubMed: 21255109]

Wheeler RJ, Gluenz E, Gull K. The limits on trypanosomatid morphological diversity. PLoS One. 2013; 8:e79581. [PubMed: 24260255]

Wheeler RJ, Scheumann N, Wickstead B, Gull K, Vaughan S. Cytokinesis in *Trypanosoma brucei* differs between bloodstream and tsetse trypomastigote forms: implications for microtubule-based morphogenesis and mutant analysis. Molecular Microbiology. 2013; 90:1339–1355. [PubMed: 24164479]

Wideman JG, Leung KF, Field MC, Dacks JB. The cell biology of the endocytic system from an evolutionary perspective. Cold Spring Harbor Perspectives in Biology. 2014; 6:a016998. [PubMed: 24478384]

Woods A, Sherwin T, Sasse R, MacRae TH, Baines AJ, Gull K. Definition of individual components within the cytoskeleton of *Trypanosoma brucei* by a library of monoclonal antibodies. Journal of Cell Science. 1989; 93(Pt 3):491–500. [PubMed: 2606940]

Woodward R, Gull K. Timing of nuclear and kinetoplast DNA replication and early morphological events in the cell cycle of *Trypanosoma brucei*. Journal of Cell Science. 1990; 95(Pt 1):49–57. [PubMed: 2190996]

Europe PMC Funders Author Manuscripts

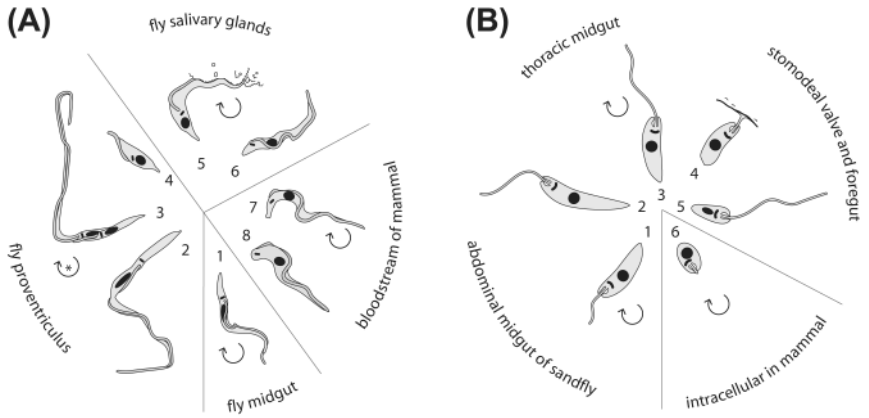

FIGURE 1. Morphological forms in the life cycle of *Trypanosoma brucei* and *Leishmania mexicana*

(A) Cell morphologies observed in the *T. brucei* life cycle. (1) Procyclic trypomastigote in the tsetse fly midgut. (2) Elongated trypomastigote, which migrates to the proventriculus where an asymmetric division (3) produces one short epimastigote (4) and one long epimastigote (thought to decay; not shown). (5) Salivary gland epimastigote. (6) Mammalian-infective metacyclic trypomastigote. (7) Long slender bloodstream form. (8) Short stumpy bloodstream form, which is preadapted to differentiate to procyclic forms following ingestion by a tsetse fly. Curved arrows denote stages undergoing proliferative cell cycles; the asterisk indicates a single asymmetric division. (B) Morphological forms in the life cycle of *L. mexicana*. (1) Procyclic promastigotes in the abdominal (posterior) midgut. (2) Slender nectomonad promastigotes, which migrate toward the thoracic (anterior) midgut. (3) Leptomonad promastigotes. (4) Broad haptomonad promastigote forms are found attached via their flagella to the chitin lining of the stomodeal valve; their precise relationship with other developmental forms is currently unclear. Leptomonad promastigotes differentiate to mammalian-infective metacyclic promastigotes (5). (6) Amastigote forms, which replicate in the phagolysosome of mammalian phagocytes. Curved arrows denote stages undergoing proliferative cell cycles.

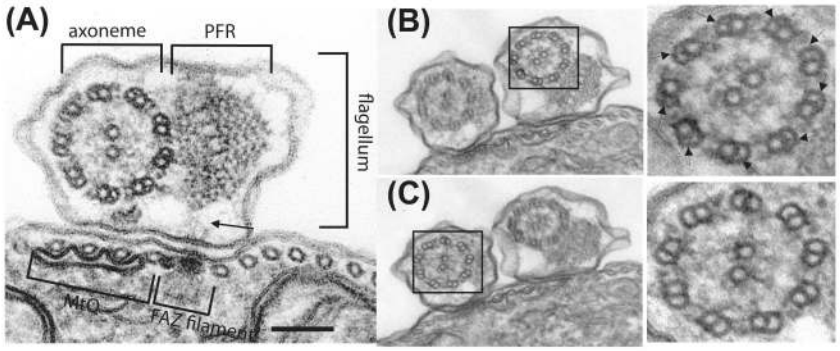

FIGURE 2. Ultrastructural characteristic of the *Trypanosoma brucei* flagellum

(A) Transverse section through a procyclic form flagellum and cell body, illustrating the 9 + 2 axoneme, PFR, and position of the FAZ filament and MtQ. (B) and (C) are the same transverse section through a cell with two flagella. The new flagellum is located to the left of the old flagellum—see text. (B) The old flagellum has been tilted on the TEM to bring the old flagellum into view. Arrowheads in the inset highlight the ponticuli within the B-tubule of each outer doublet microtubule. (C) The new flagellum has been tilted on the TEM and does not contain ponticuli. Scale bar: 100 nm.

Europe PMC Funders Author Manuscripts

Europe PMC Funders Author Manuscripts

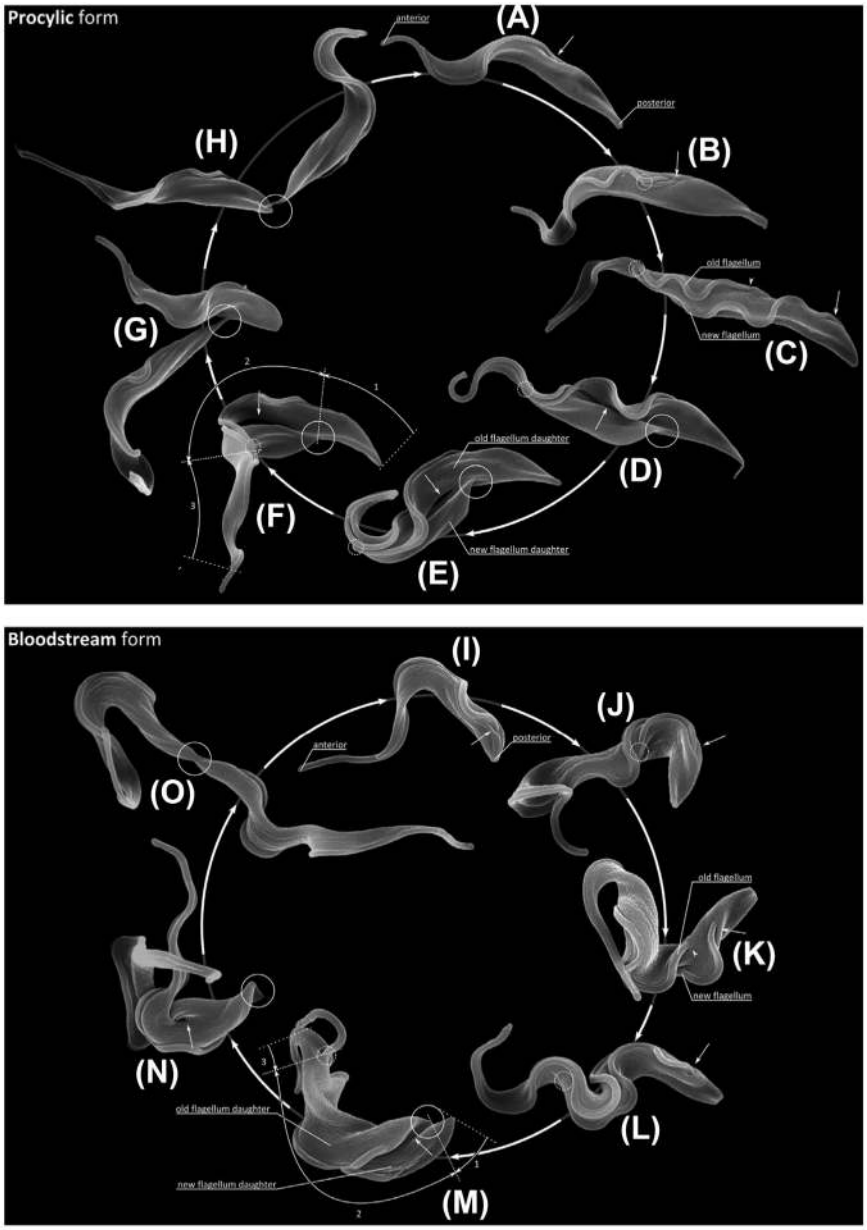

FIGURE 3. Differences in external morphology during the cell division cycle of *Trypanosoma brucei* procyclic and bloodstream forms

Composite scanning electron micrograph images of stages of procyclic (A–H) and bloodstream (I–O) form cell division. (A and I) G1 cell with a single attached flagellum. The exit point of the flagellum from the flagellar pocket is arrowed and the anterior and posterior indicated. (B and J) A new flagellum has grown to extend from the flagellar pocket (arrow). The distal tip of the new flagellum is laterally connected to the old flagellum in the procyclic form (B) and is laterally embedded in the groove structure in the flank of the cell in the bloodstream form (J), indicated by dashed circles. (C, K–L) The flagellar pocket associated with the new flagellum (arrowed) is positioned posterior to the flagellar pocket associated with the old flagellum (arrowhead). The new flagellum is located to the left of the old when

viewed looking from posterior to anterior. (D and M) A division fold is evident between the two flagella (arrowed) which is located along the long axis and begins to define the daughter cell shape. There are two distinct posterior end profiles. The new-flagellum daughter inherits the existing posterior end and a new posterior end is formed for the old-flagellum daughter (circled). The new flagellum is still attached to the old by the flagella connector in the procyclic form (D), but has grown free of the cell body in the bloodstream form (M), indicated by dashed circles. (E–F, N) A division cleft has opened up between the daughters (arrow) and the new flagellum tip remains attached to the old flagellum by the flagella connector in the procyclic form (E–F). (G–H, O) Preabscission stage. In the procyclic form (G–H) the two daughter cells are attached by the posterior end of the old-flagellum daughter (circled) to the side of the new-flagellum daughter by a cytoplasmic bridge connection. In the bloodstream form (O) a posterior-to-posterior (circled) configuration is typical (Wheeler, Scheumann, et al., 2013).

Europe PMC Funders Author Manuscripts

Europe PMC Funders Author Manuscripts

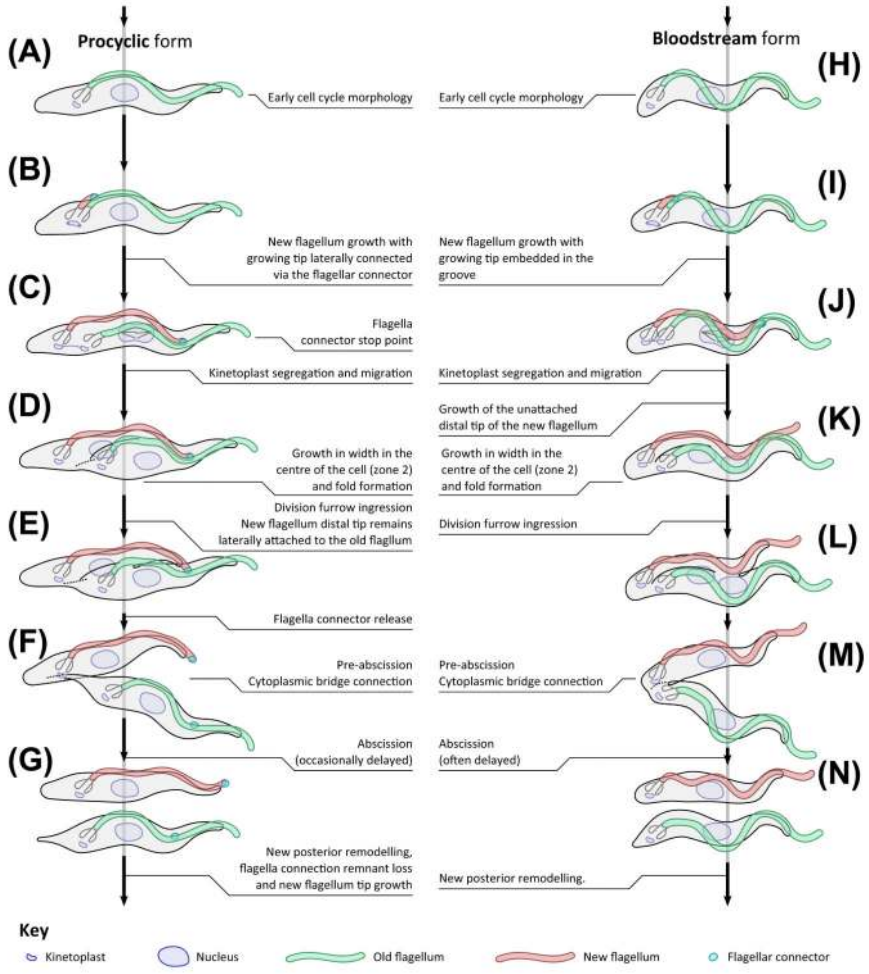

FIGURE 4. Differences in morphogenesis of the bloodstream and procyclic forms of *Trypanosoma brucei* through the cell division cycle

Major morphogenetic events are shown alongside cartoon representations of the associated cell morphologies. Vertical spacing is purely illustrative and does not represent relative time spent during each of these stages (Wheeler, Scheumann, et al., 2013).

Europe PMC Funders Author Manuscripts

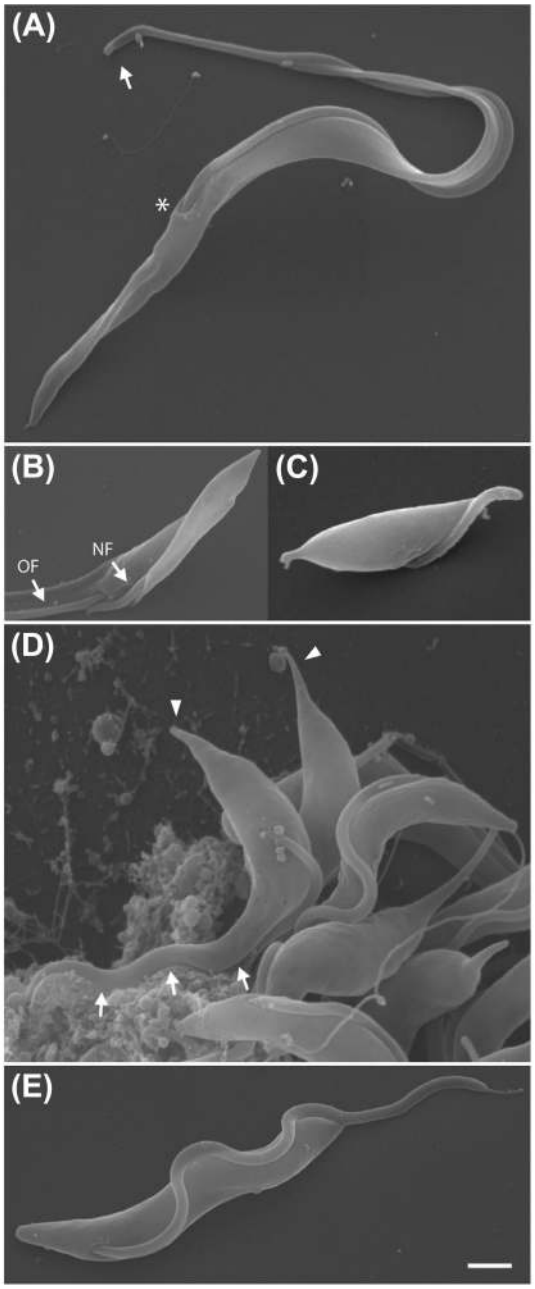

FIGURE 5. Scanning electron micrographs of trypanosome forms found in the tsetse fly proventriculus and salivary glands

(A) Long trypomastigote. The asterisk indicates the exit point of the flagellum from the flagellar pocket and the arrowhead points to the distal tip of the long flagellum. (B) Posterior end of an asymmetrically dividing cell with a clearly visible cleavage fold. Arrows point to the old (OF) and new flagellum (NF). (C) Short epimastigote found in the proventriculus. (D) Epimastigotes in the salivary gland are attached to the gland epithelium via their flagellum. Long protrusions extending from the posterior end of the epimastigote cells are marked with arrowheads. Arrows indicate the region of flagellar attachment to the tsetse salivary gland cells. (E) Metacyclic trypomastigote. Scale bar represents 1 μm.

Europe PMC Funders Author Manuscripts

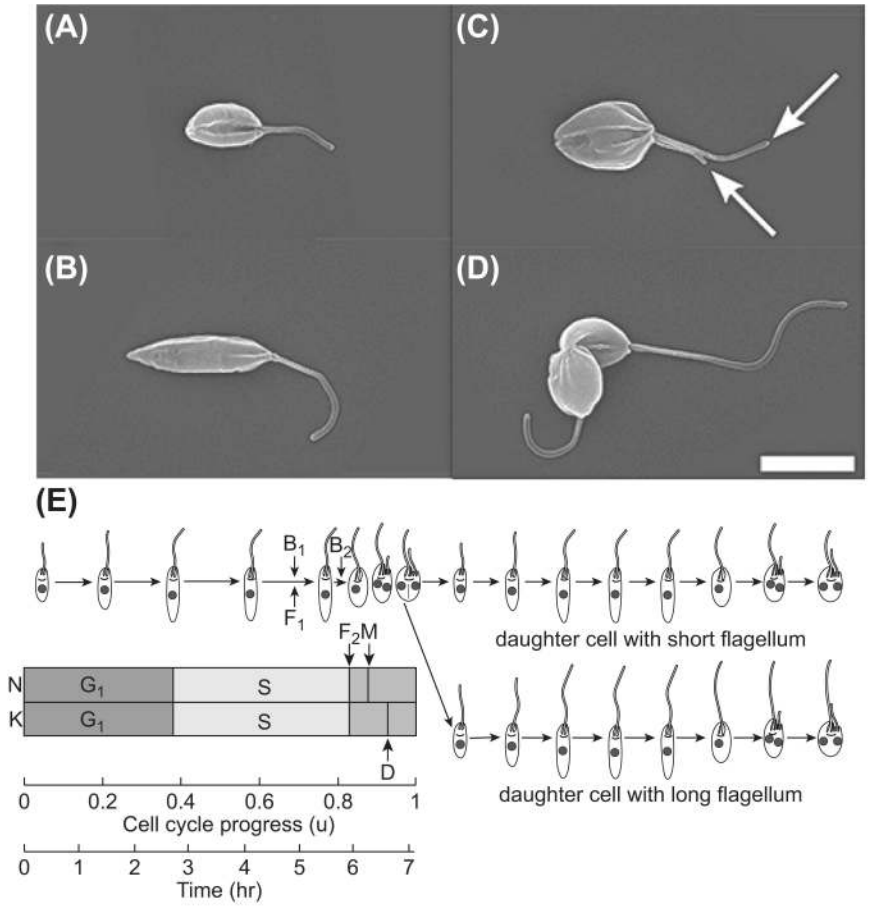

FIGURE 6. Cell cycle of *Leishmania mexicana* promastigotes

(A–D) Scanning electron micrographs showing progression of *L. mexicana* promastigote forms through the cell cycle. The arrows in (C) point to the two flagella. The scale bar represents 5 μm. (E) Cartoons of the major morphological forms during *L. mexicana* cell cycle progression and their approximate timing relative to the G1, S, and post-S phases of the nucleus [N] and kinetoplast [K]. Approximate timings are indicated for [F_1] the start of axoneme extension from the basal body, [B_1] new probasal body formation, [B_2] probasal body rotation, [F_2] emergence of the new flagellum from the flagellar pocket, [M] DNA segregation during mitotic anaphase, and [D] kinetoplast division.

Figure adapted from Wheeler et al. (2011).

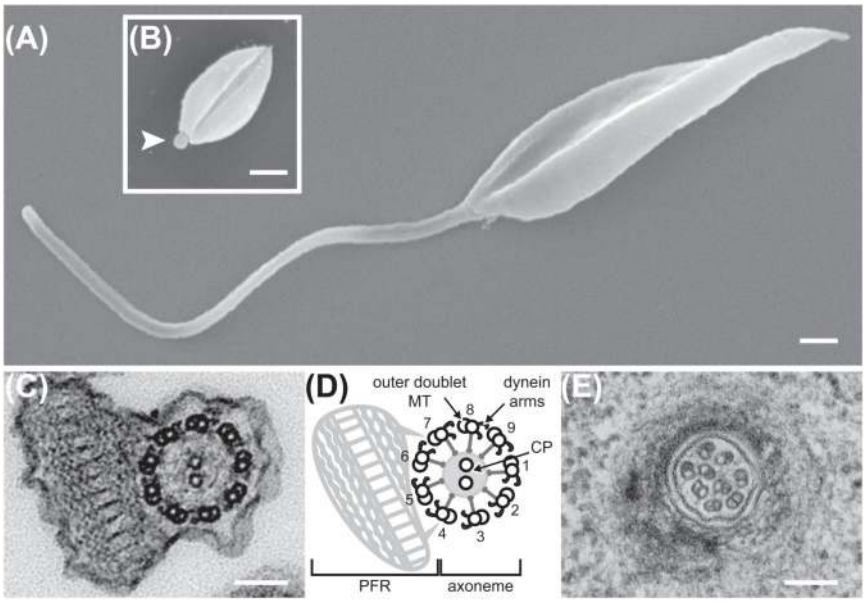

FIGURE 7. Structure of the *Leishmania* flagellum in amastigotes and promastigotes

Scanning electron micrographs show the difference in flagellum length between *Leishmania mexicana* promastigote (A) and axenic amastigote (B), where only the tip of the short amastigote flagellum is exposed to the environment (arrowhead). Differences between promastigote and amastigote axoneme architecture are clearly visible in transmission electron micrographs of flagellum cross sections (C and E, respectively). Prominent structural features of the promastigote flagellum (C) include the canonical "9 + 2" microtubule axoneme, forming a ring of nine outer microtubule (MT) doublets around a pair of central MT (CP), with associated outer and inner dynein arms, and the PFR (shown in cartoon form in D). In contrast the amastigote axoneme (E) consists of a bundle of nine doublet MT and there is no PFR. Scale bars represent 1 μm (A, B) and 0.1 μm (C–E) Figure adapted from (Gluenz, Ginger, et al., 2010).

Europe PMC Funders Author Manuscripts

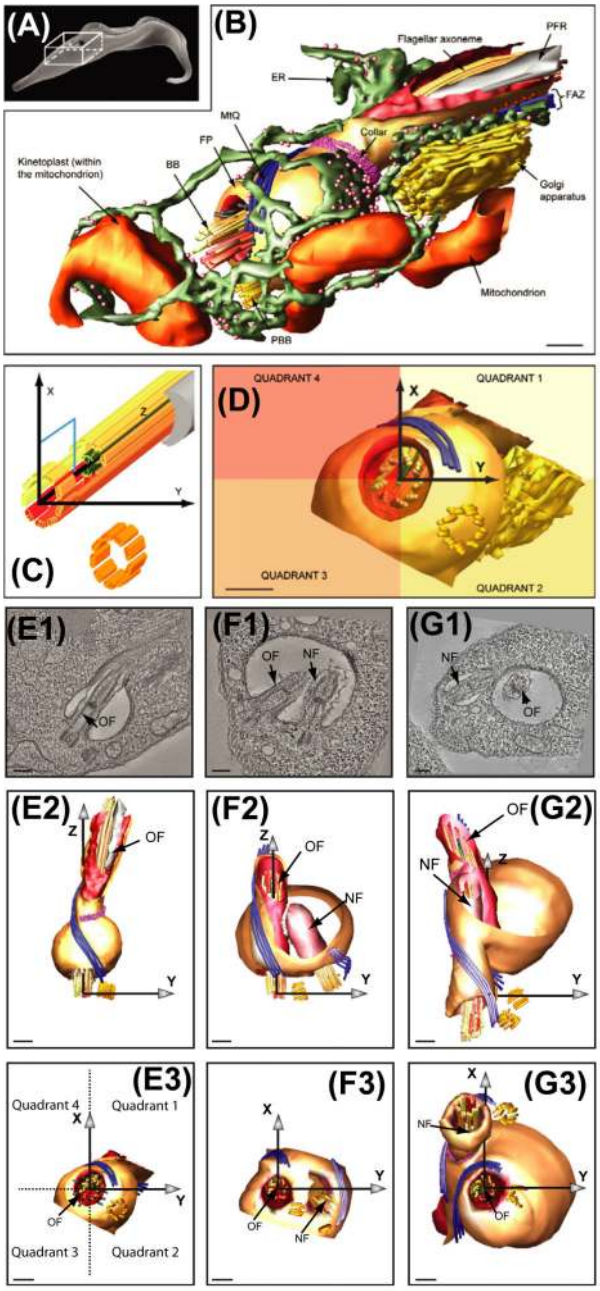

FIGURE 8. Cellular electron tomography of the *Trypanosoma brucei* flagellar pocket

(A) A scanning electron micrograph illustrates the position of the flagellar pocket region. The flagellum exit point on the cell surface is labeled with an asterisk. (B) The three-dimensional model illustrates the relationship of the cytoskeletal and membrane structures associated with the pocket. Abbreviations: BB, basal body; PBB, probasal body; FP, flagellar pocket; PFR, paraflagellar rod; MtQ, microtubule quartet; FAZ, flagellum attachment zone; ER, endoplasmic reticulum. (C) This cartoon defines the axes that we used to position tomograms. The origin point is defined by the center of the basal body at its most proximal end. The *z*-axis runs up the length of the axoneme; the *x*-axis is defined by the

plane of the central pair microtubules at the point at which they are nucleated; finally, the *y*-axis points toward the probasal body. (D) A model with many of the components excluded has been orientated such that the view is along the *z*-axis. This allows the definition of four quadrants in the cell useful for positioning organelles and structures and comparison of tomograms. Scale bars: 200 nm (Lacomble et al., 2009). Three representative tomograms (E–G) reveal different stages of basal body and flagellar pocket morphogenesis and demonstrate the rotation. (E1, F1, and G1) show slices through the flagellar pockets from the original tomograms. Tomogram models (E2,3) contain the Cartesian axes described above (Lacomble et al., 2009). (E2,3) Two views of the model of a tomogram illustrating a cell in which the probasal body is located on the bulge side of the flagellar pocket in quadrant 2. The origin of the microtubule quartet lies between the two basal bodies. (F2,3) In this cell, the probasal body has matured and has subtended a new flagellum (NF) that has invaded the existing flagellar pocket and connected to the old flagellum (OF). The new flagellum is still positioned essentially as in (E2 and 3): quadrant 2. (G2,3) A later stage in the cell cycle just before flagellar pocket division. The new flagellum is now in a more posterior location and lies in quadrant 4 (Lacomble et al., 2010). (See color plate)

Europe PMC Funders Author Manuscripts

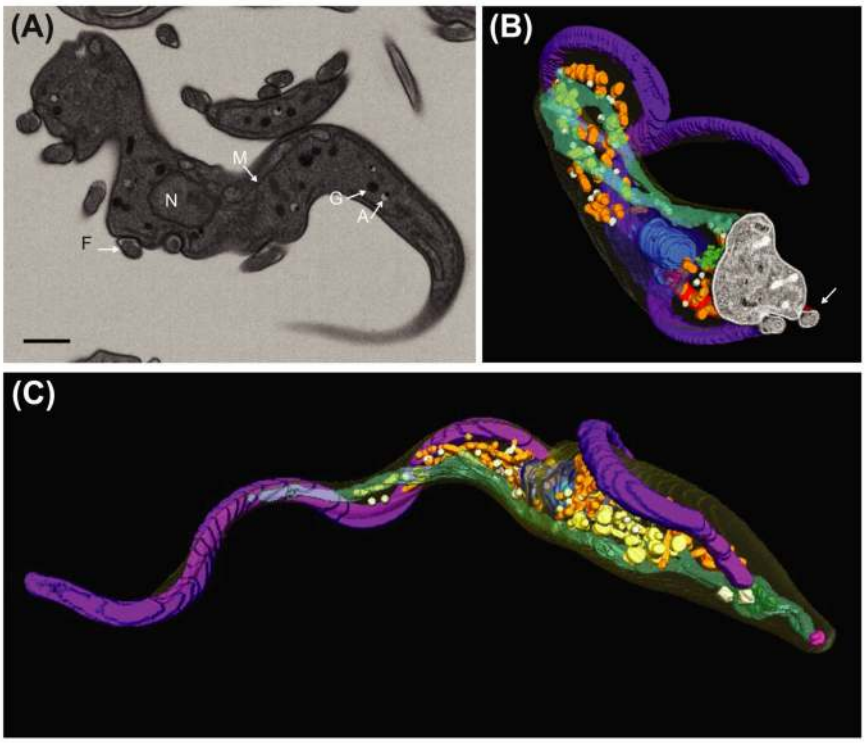

FIGURE 9. SBFSEM of bloodstream form *Trypanosoma brucei*

(A) A single slice (100 nm thick) from an SBFSEM dataset, illustrating organelles and cytoskeletal structures of the cell. (B) Surface volume rendering of the SBFSEM dataset containing a whole cell with a transverse slice from the dataset to illustrate the rendering process. (C) A whole-cell rendering of a G1 cell. Index: mitochondrion (M)—green; nucleus (N)—blue; old flagellum (F)—purple; new flagellum (arrow in B)—red; glycosomes (G)—orange; acidocalcisomes (A)—white; vesicles—yellow. Scale bar: 500 nm. (See color plate)

Europe PMC Funders Author Manuscripts

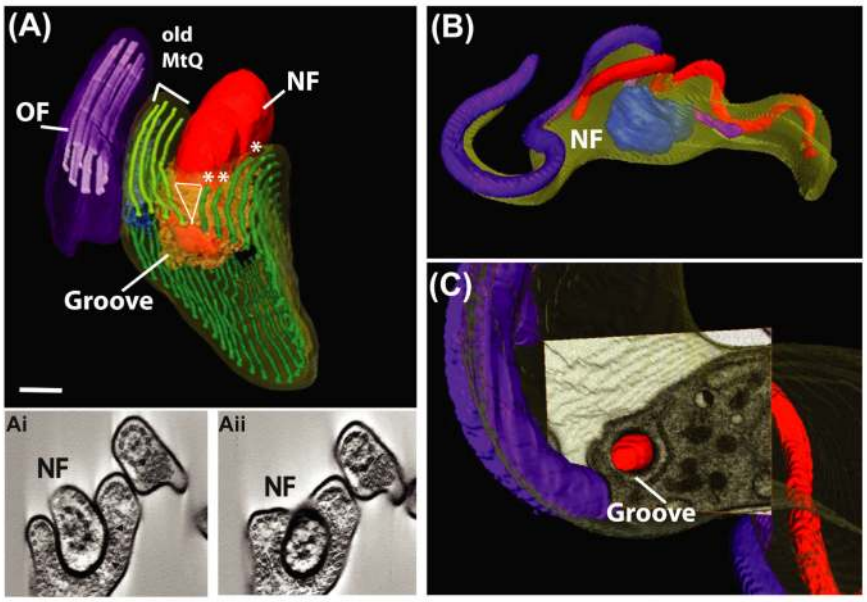

FIGURE 10. Combining cellular electron tomography and SBFSEM to analyze the ultrastructure of the groove

(A) Surface rendering of segmented data illustrating the location of the distal tip of the new flagellum in an indentation of the cell body membrane called the groove. Subpellicular microtubules (green) surround the groove and there is close association of the old MtQ with the groove. (Ai, Aii) Selected *z*-slices of the tomogram ~6 nm thick in (A). Index: old flagellum (OF)—purple; new flagellum (NF)—red; subpellicular microtubules—green; MtQ—light green. Asterisks illustrate short microtubules that finish in the tomogram; (B) surface rendering of a whole cell to illustrate the distal tip of the new flagellum located inside the cell body; (C) same cell as (B) with a slice from the SBFSEM data to illustrate the groove. Scale bar: 200 nm. (See color plate)

Europe PMC Funders Author Manuscripts